A study on the magnetic behavior of Nd-Fe-B/α-Fe nanocomposite films

Journal of Physics: Conference Series **232** (2010) 012014 doi:10.1088/1742-6596/232/1/012014

A study on the magnetic behavior of Nd-Fe-B/α-Fe nanocomposite films

S Madeswaran[1], S Tamano[2], S Goto[2] and K Tokiwa[1,2]

[1]Polyscale Technology Research Center, Tokyo University of Science
2641 Yamazaki, Noda, Chiba 278-8510, Japan

[2]Department of Applied Electronics, Tokyo University of Science, Japan
2641 Yamazaki, Noda, Chiba, 278-8510, Japan

E-mail: smades@rs.noda.tus.ac.jp

Abstract. Nanocomposite Nd-Fe-B / α-Fe thin films were prepared by sputtering successively a Nd-rich $Nd_{21}Fe_{64}B_{15}$ and a Fe targets in a multilayer structure using radio frequency (RF) magnetron gun. We have studied the influence of thickness of α-Fe layer on the magnetic properties of Nd-Fe-B / α-Fe thin films. A nanocomposite thin film with 15nm thick α-Fe layer prepared on 550˚C heated substrate gives the highest energy product, 190 kJ/m^3 along with a coercivity of 950 kA/m. Magnetic hysteresis loop measurement shows that the hard (Nd-Fe-B) and soft (α-Fe) layers are exchange coupled firmly for the films deposited on heated substrate whereas the two layers are decoupled for room temperature deposited and post annealed films.

1. Introduction

Nanocomposite materials, consisting of a fine mixture of a magnetically soft phase with high magnetization exchange coupled to a high anisotropy hard phase have been widely studied due to their application as high energy product and low cost permanent magnets [1-7]. A vital efforts are being performed by several researchers to increase the energy product, BH_{max}, in permanent magnet in the form of bulk [1-2] as well as in thin film [5-7]. However the practical values of remanence and maximum energy product are much lower than the theoretical values predicted by micromagnetic calculations [3-4] for nanocomposite having ideal exchange coupling between the grains of two phases. The main reason for such low values is due to large difference between ideal and practical grain size and distribution, and especially crystalline orientation of hard phase. Films based on a tetragonal $Nd_2Fe_{14}B$ phase are obviously the potential candidates because it possesses superior hard magnetic properties such as high spontaneous magnetization and large coercivity [1-2, 5-7]. Thin films of Nd-Fe-B with α-Fe nanocomposite magnets prepared by sputtering deposition in tri-layer form [5] with the soft layer sandwiched between the two hard magnetic layers showed enhanced remanence. The understanding of such multilayer system in the thin film is of considerable interest since the properties of sample could be optimized by controlling the thickness of each layer. Furthermore, the Nd-rich phase in connection with $Nd_2Fe_{14}B$ phase leads to higher coercivity with preferred orientation [8-10]. We therefore investigated Nd-rich Nd-Fe-B multilayer with soft magnetic (α-Fe) layer combination.

2. Experiment

Thin films of layer structure, Ta (35nm) /NdFeB (120nm)/ α-Fe (x nm)/ NdFeB (120nm)/Ta(20nm) where x = 0, 15, 30 60 and 90, were deposited by sequential sputtering of Ta (50mm Ø x 5mm size), Nd-rich with a nominal composition of $Nd_{21}Fe_{65}B_{14}$ (50mm Ø x 2mm) and Fe (50mm Ø x 0.1mm) targets onto glass substrate in a multiple gun RF plasma chamber with a base pressure of ~$8x10^{-5}$ Pa. The $Nd_{21}Fe_{65}B_{14}$ target was prepared by arc melting in an Ar atmosphere and successive spark plasma sintering (sintering temperature 700˚C and pressure 30kN) after well ground the ingot. The Ta buffer layer used here is to enable texturing of $Nd_2Fe_{14}B$ phase and also to prevent diffusion of substrate materials into the film [11]. A set of samples were prepared directly on heated substrate at 550˚C and the samples will be referred to as type-I. Another set of multilayer were made by depositing hard (NdFeB) and soft (Fe) magnetic layer at room temperature while Ta buffer layer deposited at 550˚C to maintain crystalline buffer phase with (110) orientation for consistency of growth interface of hard magnetic layer. After deposition at room temperature the samples were annealed at 650˚C for 15 min in an Ar atmosphere (where the O_2 content is reduced to 10^{-22} torr with the help of oxygen controller, STLab SiOC-200DC, connected with annealing furnace) to crystallize both the phases. These post annealed samples will be referred to as type-II. For all experiment, the deposition conditions such as pressure of Ar (high purity) gas, sputter power and distance between target and substrate were sustained at 5 Pa, 130 W and 60mm, respectively. X-ray diffraction (XRD) analysis was performed with a Rigaku Ultima-III diffractometer utilizing Cu-Kα radiation. Microstructural investigations were performed with a JEOL (JSM-7001F) field emission scanning electron microscope (FE-SEM). Magnetic properties were measured in both perpendicular and parallel direction to the film plane by vibrating sample magnetometer (VSM) with a maximum field of 20 kOe.

3. Results and Discussion

The XRD patterns of type-I films with layer form Ta(35nm)/NdFeB(240nm)/Ta(20nm), Ta (35nm) /NdFeB (120nm)/ α-Fe (15 nm)/ NdFeB (120nm)/Ta(20nm) and Ta (35nm) /NdFeB (120nm)/ α-Fe (60 nm)/ NdFeB (120nm)/Ta(20nm) are shown in figure 1. For the films deposited with and without α-Fe layer, intensity peaks corresponding *(004), (006)* and *(008)* plane of crystalline $Nd_2Fe_{14}B$ phase occur with a strong (*00l)* texture, that is, c-axis tending to be perpendicular to the film plane. After introducing a 15nm thick α-Fe layer in hard magnetic layer like sandwich structure and increasing its thickness further, the XRD patterns show increasing trend of intensity of the peak presents at 44.6˚, which can be attributed to main reflection of α-Fe phase superimpose with *(006)* peak of $Nd_2Fe_{14}B$, and indicating the increase of α-Fe phase in the film. It is also interesting to note that intensities of peaks appearing at 30.3˚ and 50.7˚ assigned for Nd-rich and Nd_xO_y phases are decreasing for increase of thickness of α-Fe layer. The decrease of Nd-rich phase is comparable to the speculation made by Kato et al [6] who specified that Nd-rich phase depends on volume fraction of Fe, and its relative concentration in the film decreases with increasing volume fraction of Fe. The Nd-rich phase usually consists of complex Nd containing intermetallic compound and Nd_xO_y [12-13]. Additionally, the x-ray results show a unknown intensifying peak (at 35.2˚ - marked as * in pattern) with respect to α-Fe layer thickness and this is presumably due to the presence of Fe_3B, $Nd_1Fe_4B_4$ and Fe_x Nd_y.

Figure 2 shows the XRD patterns of type-II films, Ta/NdFeB/α-Fe (x) /NdFeB/ Ta with x = 0, 15 and 30 nm. The annealing for these films was performed rapidly with a ramp rate of 150˚C/Sec according to the reports [14-15] that showed enhanced magnetic properties for rapid thermal annealed NdFeB thin films compared with a long time anneal as the rapid thermal temperature rise leads to more nucleation centers. The x-ray diffraction analyses of these films show the evidence of $Nd_2Fe_{14}B$ phase at the same time the preferred c-axis orientation of Nd-Fe-B film is not vertical to the film plane since there are many peaks with exclusion of definite intensity of (*00l*) crystalline planes. It is believed that the Nd_xO_y phase might support the growth of $Nd_2Fe_{14}B$ phase with c-axis texture when the deposition temperature is high; however, it obstructs the growth of texturing $Nd_2Fe_{14}B$ phase at low deposition temperatures and subsequent annealing treatment [16-17].

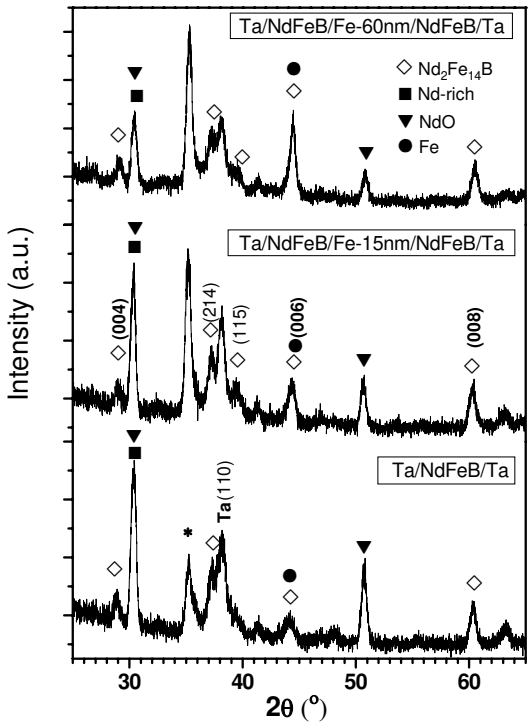

Figure 1. XRD patterns of the films deposited at 550˚C.

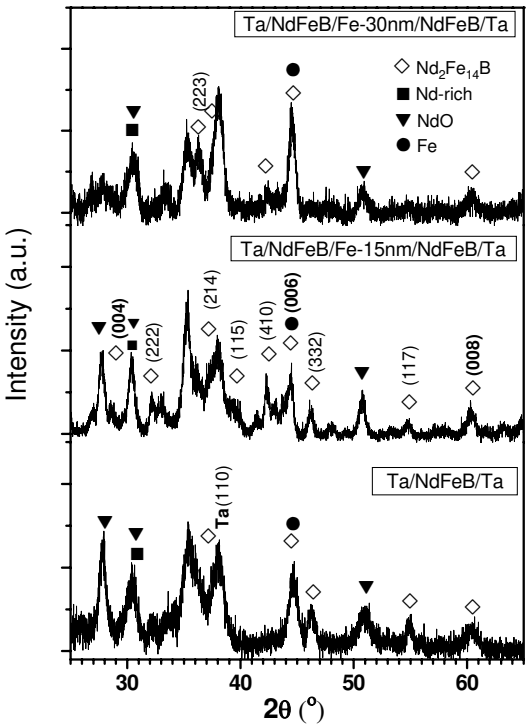

Figure 2. XRD patterns of the films deposited at room temperature and post annealed at 650˚C.

To study about the grain growth, a film in the form of Ta/NdFeB(240nm)/Fe(30nm) was developed at high temperature (550˚C) and analyzed by FE-SEM. Figure 3a shows FE- SEM image of this sample surface. The grains are irregular rectangular like shape and the average gain size is about 90 nm. Figure 3b displays a compositional mapping of the same area of (a). In this imaging mode, the gray contrast arises from the α-Fe phase, while the white contrasts arise from the $Nd_2Fe_{14}B$ phase. From this image the approximate grain size of α-Fe is estimated around 30 nm. Compositional mapping were also observed at cross sectional view of type-I and type-II films and are shown in figure 3c and d, respectively. The α-Fe layer or grains could not be seen in type-I sample whereas in the case type-II the image displays a clear thick gray line corresponding to the α-Fe phase. From the images 3b, c and d, it can be said that the α-Fe grains in type-I are embedded well in the Nd-Fe-B matrix compared with type-II film. FE-SEM imaging observation also infers that the type-I films are always having higher roughness compared with type-II because of higher atomic mobility at high temperature deposition.

The magnetic behavior at room temperature of type-I films are shown in the left column of figure 4. The solid and dashed lines represent measuring field direction along perpendicular (out-plane-⊥) and parallel (in-plane-||) to the film plane, respectively. Demagnetization correction has not been performed for any of the measurement. The single phase like hysteresis loops for these samples measured along perpendicular direction have no two-step demagnetization process indicating that the soft and hard phases are exchange coupled. Moreover, the out-plane magnetization values are always larger than the in-plane, implying a good alignment of $Nd_2Fe_{14}B$ grains in c-axis which is consistent with x-ray diffraction data displayed in figure 1.

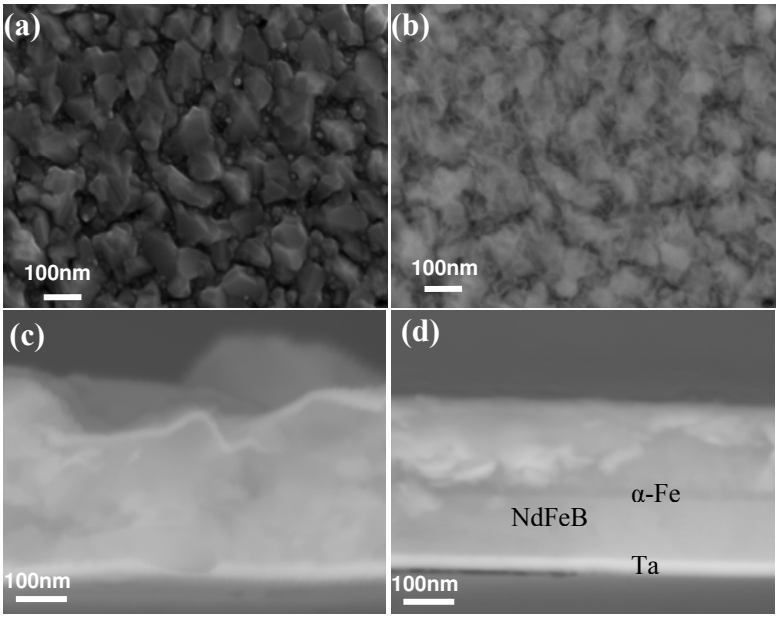

Figure 3. (a) FE-SEM image of Ta/NdFeB(240nm)/ α-Fe(30nm) film developed at 550˚C, (b) compositional mapping of area (a), (c) Cross sectional view of Ta/NdFeB/α-Fe/NdFeB/Ta film of type-I and (d) type-II.

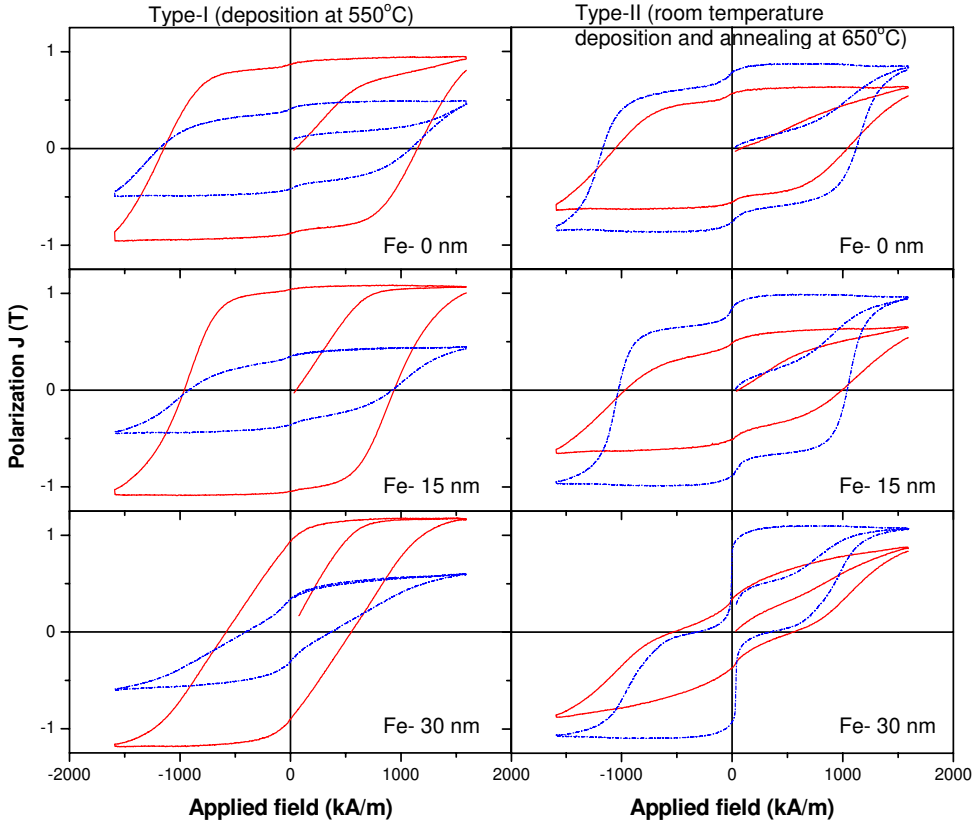

Figure 4. Room temperature hysteresis loops of type-I (left column) and type-II samples (right column) in the form of Ta(35nm)/NdFeB(120nm)/ α-Fe(*x* nm) /NdFeB(120nm) /Ta(20nm) with *x* =0, 15 and 30 (Solid curves : *H*⊥ film plane, dotted curves *H* || film plane).

The right column of figure 4 represents the magnetic properties of type-II samples. The NdFeB layer without α-Fe phase show a kink near zero applied field indicating the existence of secondary phase and this result coincides with the investigation made by Tokumaru et al [18]. For the addition of α-Fe layer, the two-step demagnetization process is pronouncing well and the step length drastically increases depending on α-Fe layer thickness. It obviously deduces that the soft and hard phases are decoupled, that is, there is poor exchange coupling between the phases presented in the film. Another point to note worth is that this type of samples exhibit larger in-plane magnetization values compared with out-plane. This is in agreement with X-ray patterns showed in figure 2 and suggesting that the easy magnetization axis is along the film plane.

Figure 5 summarizes the saturation magnetization (J_s), coercivity (H_c), maximum energy product (BH_{max}) and remanence ratio (J_r/J_s) of type-I sample as a function of α-Fe layer thickness. As described by many researchers [6, 13-14], who studied magnetic behavior against volume fraction of soft phase, it can obviously be seen that magnetization decreases and coercivity increases with increasing soft layer thickness. The J_s increases with the Fe content as one would expect since Fe has a larger moment (per gram) than NdFeB. The H_c decreases rapidly from 1150 kA/m to 950 kA/m for adding 15nm thick α-Fe layer since this composite system now has a smaller anisotropy per unit volume. These two opposition factors enable the maximum energy product to peak point at 15 nm thick α-Fe layer. The remanence ratio is higher for 15 nm and it is decreasing with further increase of thickness, indicating the deterioration of formation of $Nd_2Fe_{14}B$ crystallographic texturing. This deterioration may arise from the distribution of shape and size of grains. As a result, the maximum of BH_{max} value of 190 kJ/m^3 can be achieved for a nanocomposite film with 15nm α-Fe layer. However, the obtained maximum BH_{max} is smaller than the reported values of isotropic nanocomposite [2], this is mainly because of small magnetization value caused by the presence of non-magnetic phases as depicted by X-ray diffraction (figure 1). For the film of Ta/NdFeB(240nm)/Fe(30nm) layer which is subjected to compositional mapping (figure 3b), the magnetic behavior is more or less same as the tri-layer film in the form of Ta/NdFeB(120nm)/ α-Fe(30 nm)/NdFeB(120nm)/Ta.

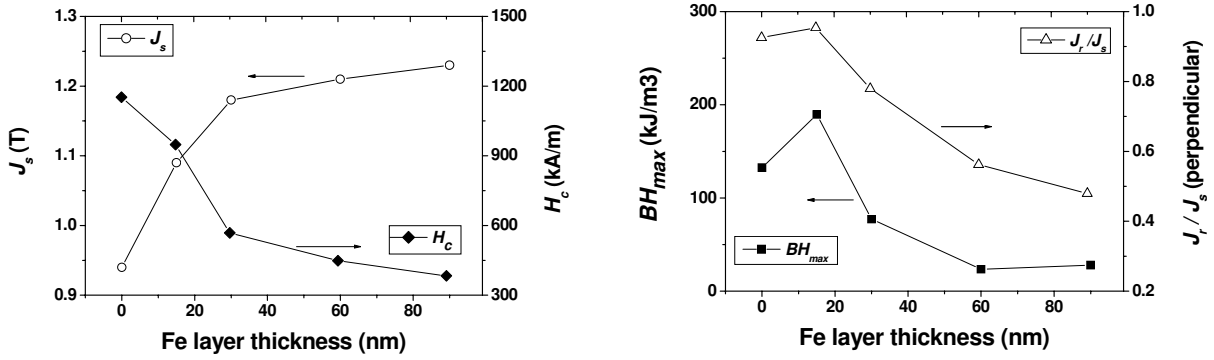

Figure 5. Magnetic properties of Ta(35nm)/NdFeB(120nm)/ α-Fe(x nm)/NdFeB(120nm)/Ta(20nm) (x =0, 15, 30, 60, 90) thin films (type-I) with different thickness of Fe layer.

4. Conclusion

The effect of α-Fe layer thickness on the magnetic properties and exchange coupling interaction of hard-soft-hard magnetic tri-layers of type-I (deposited at 550˚C), and type-II (room temperature deposition and being annealed at 650˚C for 15 min), were investigated. The results show that α-Fe layer is fully coupled to the Nd-Fe-B phase and nanocomposite structure can be developed for type-I films. The exchange coupled tri-layer with 15nm thick α-Fe gives a significant magnetic properties: H_c=950 kA/m, J_r = 1.04 T, $(BH)_{max}$ = 190 kJ/ m^3 (23.8 MGOe). If we increase the thickness of α-Fe

layer to 30nm, the coercivity is greatly decreased to 570 kOe and texturing of the magnetic film also starts to deteriorate. Type-I films exhibit easy magnetization axis along perpendicular to film plane, where as type-II exhibit easy magnetization axis along film plane with decoupling between hard and soft phases.

Acknowledgement
This research work was supported by "Academic Frontier" Project for Private Universities: matching fund subsidy from MEXT (Ministry of Education, Culture, Sports, Science and Technology), 2006-2010.

References:

[1] Bauer J, Seeger M, Zern A, and Kronmuller H 1996 *J. Appl. Phys.* **80** 1667
[2] Liu S, Higgins A, Shin E, Bauser S, Chen C, Lee D, Shen Y and Huang M Q 2006 *IEEE Trans. Magn.* **42** 2912
[3] Kneller E F and Hawig R 1991 *IEEE Trans. Magn.* **27** 3588
[4] Skomski R and Coey J M D 1993 *Phys. Rev. B* **48** 15812
[5] Shindo M, Ishizone M, Kato H, Miyazaki T and Sakuma A 1996 *J. Magn. Magn. Mater.* **161** L1
[6] Kato H, Ishizone M, Koyama K and Miyazaki T 2005 *J. Magn. Magn. Mater.* **290-291** 1221
[7] Cui W B, Zheng S J, Liu W, Ma X L, Yang F, Yao Q, Zhao X G and Zhang Z D 2008 *J. Appl. Phys.* **104** 053903
[8] Makita K and Yamashita O 1999 *Appl. Phys. Lett.* **74** 2056
[9] Watanabe N, Umemoto H, Itakura M, Nishida M and Machida K 2009 *IOP Conf. Series: Mater. Sci. Eng.* **1** 012033
[10] Madeswaran S, Tokumaru R, Tamano S, Goto S, Tokiwa K and Watanabe T 2009 *J. Phys.: Conf. Series* **191** 012024
[11] Hannemann U, Fähler S, Oswald S, Holzpfel B and Schultz L 2002 *J. Magn. Magn. Mater.* **242** 1294
[12] Minowa T, Shimao M, Honshima M 1991 *J. Magn. Magn. Mater.* **97** 107
[13] Yue M, Zhang J X, Liu W Q and Wang G P 2004 *J. Magn. Magn. Mater.* **271** 364
[14] Jiang H and O'Shea N J 2000 *J. Magn. Magn. Mater.* **212** 59
[15] Kojima A, Makino A and Inoue A 2000 *J. Appl. Phys.* **87** 6576
[16] Chen S L, Zheng J G, Liu W and Zhang Z D 2007 *J. Phys. D: Appl. Phys.* **40** 1816
[17] Serrona L K E B, Sugimura A, Adachi N, Okuda T, Ohsato H, Sakamoto I, Nakanishi A, Motokawa M, Ping D H and Hono K 2003 *Appl. Phys. Lett.* **82** 1751
[18] Tokumaru R, Tamano S, Goto S, Madeswaran S, Tokiwa K and Watanabe T 2009 *J. Phys.: Conf. Series* **191** 012021